NANO · MICRO small
www.small-journal.com

Rational Design of the Alkali Metal Sn-Based Mixed Halides with Large Birefringence and Wide Transparent Range

Junbo Wang, Mengmeng Zhu, Yaoqing Chu, Jindan Tian, Lili Liu, Bingbing Zhang,* and P. Shiv Halasyamani**

Birefringent materials are widely used in various advanced optical systems, owing to their vital role in creating and controlling polarized light. Currently, Sn^{2+}-based compounds containing stereochemically active lone-pair (SCALP) cations are extensively investigated and considered as one class of promising birefringent materials. To solve the problem of relatively narrow bandgap of Sn^{2+}-based compounds, alkali metals and multiple halogens are introduced to widen the bandgap during the research. Based on this strategy, four new Sn^{2+}-based halides, $A_2Sn_2F_5Cl$ and $ASnFCl_2$ (A = Rb and Cs), with large birefringence, short ultraviolet (UV) cutoff edge, and wide transparent range are successfully found. The birefringences of $A_2Sn_2F_5Cl$ (A = Rb and Cs) are 0.31 and 0.28 at 532 nm, respectively, which are among the largest in Sn-based halide family. Remarkably, $A_2Sn_2F_5Cl$ possess relatively shorter UV cutoff edge (<300 nm) and broad infrared (IR) transparent range (up to 16.6 µm), so they can become promising candidates as birefringent materials applied in both UV and IR regions. In addition, a comprehensive analysis on crystal structures and structure–property relationship of metal Sn^{2+}-based halides is performed to fully understand this family. Therefore, this work provides insights into designing birefringent materials with balanced optical properties.

1. Introduction

Birefringence is the largest difference of refractive index under different polarization conditions relating to the total optical anisotropy polarization of the structure, which is one of the essential properties of optoelectronic functional crystals, especially for birefringent materials.[1] Due to the capacity of modulating the polarization of light, birefringent materials are widely used as polarizers, optical isolators, and circulators in the fields of optical communication and laser industries.[2] In the last few decades, some commercial birefringent crystals that can be used in optical regions from the UV region to IR region have been discovered, such as $CaCO_3$,[1a] YVO_4,[3] MgF_2,[4] α-BaB_2O_4,[2a] and so on. However, these birefringent materials still have defects, such as small birefringence, difficulty in crystal growth, and low UV transmittance, that limit their practical application.[5] It is highly challenging to find new birefringent materials with balanced overall performances, especially broad bandgap and large birefringence.

According to the relationship between structures and properties, the birefringence of a compound depends on the optical anisotropic polarizability, that is, related to basic functional modules and their spatial arrangement.[6] In general, planar structural groups with π-conjugation (like inorganic units[7] $[BO_3]^{3-}$, $[CO_3]^{2-}$, $[NO_3]^{-}$, and organic units[8] $[H_{3-x}C_3N_3O_3]^{x-}$ ($x = 1$–3), etc.) have been widely studied and reported as popular groups to construct UV birefringent crystals due to their ability to induce strong anisotropic polarizability and high UV transmittance. However, the generation of large birefringence must request either the layer arrangement or the coaxial arrangement of π-conjugated planar groups. Otherwise, it will get a small birefringence. To date, many excellent birefringent crystals based on π-conjugate groups have been reported, such as $Ca(BO_2)_2$ (0.247 at 193 nm, 7.34 eV),[7a] $Na_3Rb_6(CO_3)_3(NO_3)_2Br{\cdot}6H_2O$ (0.165 at 1064 nm, 4.8 eV),[7c] $SrAlB_3O_6F_2$ (0.078 at 1064 nm, 7.65 eV),[7d] $LiZn(OH)CO_3$ (0.147 at 1064 nm, 6.53 eV),[9] $Sc(IO_3)_2(NO_3)$ (0.366 at 546 nm, 4.15 eV),[10] $KLi(HC_3N_3O_3){\cdot}2H_2O$ (0.186 at 514 nm, 5.23 eV),[8a] $Cd(H_2C_6N_7O_3)_2{\cdot}8H_2O$ (0.6 at 550 nm, 4.0 eV),[8b] and $Ca(H_3C_4N_2O_3)_2{\cdot}H_2O$ (0.49 at 546.1 nm, 3.61 eV).[8c] In addition, SCALP cations (such as Sn^{2+}, Bi^{3+}, Sb^{3+}, and Pb^{2+}) always exhibit large optical anisotropy induced by second-order Jahn–Teller (SOJT) effect, and they are more propitious to generate large birefringence due to the relatively lower requirement for their spatial arrangement.[11] Recently,

J. Wang, M. Zhu, Y. Chu, J. Tian, L. Liu
Institute of Crystal Growth
School of Materials Science and Engineering
Shanghai Institute of Technology
Shanghai 201418, China
E-mail: liulili@sit.edu.cn
B. Zhang
College of Chemistry and Environmental Science
Hebei University
Baoding 071002, China
E-mail: zhangbb@hbu.edu.cn
P. S. Halasyamani
Department of Chemistry
University of Houston
112 Fleming Building, Houston, TX 77204, USA
E-mail: psh@uh.edu

The ORCID identification number(s) for the author(s) of this article can be found under https://doi.org/10.1002/smll.202308884

DOI: 10.1002/smll.202308884

by introducing different SCALP cations, many compounds with sufficiently large birefringence have been reported, such as $RbCl{\cdot}(H_2SeO_3)_2$ (0.14 at 1064 nm),[12] $Sc(HSeO_3)_3$ (0.105 at 1064 nm),[13] $(NH_4)_2(I_5O_{12})(IO_3)$ (0.431 at 546 nm),[13] Sn_2PO_4I (0.468 at 1064 nm),[11c] $Sn_{14}O_{11}Br_6$ (0.265 at 546 nm),[11d] and SbB_3O_6 (0.318 at 546 nm).[14]

Metal oxides are generally difficult to apply in the IR region owing to their intrinsic short IR absorption edges, that are attributed to the higher bond stretching frequency in oxo-metal anionic groups.[15] Attributable to the relatively large bandgap and wide optical transparency window, the metal halides, as a type of non-oxygen compounds, have received increasing attention in the fields of nonlinear optical crystals and birefringent crystals.[16] Many metal halides with excellent optical performances have been reported, such as α-SnF_2 (0.191 at 546 nm, 276 nm),[17] $HgBr_2$ (11 × KDP, 0.24 at 1064 nm, 0.38–30 μm),[18] $RbSn_2Cl_5$ (0.102 at 1064 nm),[19] and $Cs_2Hg_3I_8$ (15 × KDP, 0.095 at 1064 nm, 0.5–25 μm).[20] The introduction of different types of halogen anions into one crystal structure is also a strategy to design compounds with diverse structures and improved optical properties. On the one hand, multiple types of halogen anions can promote the formation of different fundamental building blocks (FBBs). On the other hand, synergistic effect of multiple halogen ions can influence the chemical bonds and enhance the structural distortion of FBBs, then to optimize linear and nonlinear optical performances of materials. For example, compared to Cs_2HgI_4, the bandgap of mixed halide $Cs_2HgI_2Cl_2$ extends from 2.34 eV to 3.15 eV; compared to $RbCdI_3{\cdot}H_2O$, the second harmonic generation (SHG) effect of mixed halide $Rb_2CdBr_2I_2$ is enhanced from 3.6 × KDP to 4 × KDP.[21]

Sn^{2+} cation is an excellent birefringence active ion due to its stereochemically active lone pairs, which can cause large structural distortion and enhance optical anisotropy. However, Sn^{2+}-based compounds have intrinsically narrow bandgap. It is particularly important to maintain a balance between large birefringence and broad bandgap for birefringent materials. Therefore, alkali metals and alkaline earth metals (lack of electron transitions of d–d and f–f orbitals) are the preferential choices to be introduced into Sn^{2+}-based system, then to explore new birefringent crystals with desirable UV bandgap.[30]

Considering above ideas, we concentrate on the exploration of the alkali metal Sn^{2+}-based mixed halide system in this study. Based on the investigation of the Inorganic Crystal Structure Database (ICSD version 5.1.0, the last release of ICSD-2023.2), there are several compounds have been found in this system, but their optical properties are rarely studied (Table 1). In this work, four new alkali metal Sn^{2+}-based halides, $A_2Sn_2F_5Cl$ and $ASnFCl_2$ (A = Rb and Cs), were obtained through hydrothermal method. These four compounds exhibit large birefringence (0.06–0.31 at 532 nm), wide bandgap (4.05–4.43 eV), and broad IR transparent region (up to 16.6 μm). Especially, the $Rb_2Sn_2F_5Cl$ and $Cs_2Sn_2F_5Cl$ have the largest birefringence in Sn-based halide family, and the birefringence values are 0.31 and 0.28 at 532 nm, respectively. Therefore, $A_2Sn_2F_5Cl$ amazingly combine large birefringence, broad bandgap, and wide transparent range together, which make them more competitive as birefringence crystals in UV–vis–IR region, particularly in IR region. Above data indicate that birefringent crystals with well-balanced optical properties can be achieved through the interactions among alkali metal cations, SCALP cations, and multiple halogen atoms.

Table 1. Compounds in alkali metal Sn^{2+}-based mixed halide system. Δn is birefringence.

Compounds	Space group	Bandgap [eV]	Δn at 1064 [nm]	SHG [×KDP]	References
$K_3Sn_5Cl_3F_{10}$	*Cmcm*	/	0.173[19]	/	[22]
$Na_3Sn_2F_6Cl$	$R\bar{3}c$	3.88	0.183[19]	/	[23]
$Cs_3Sn_3F_2Cl_7$	$P2_1/c$	2.96	/	/	[24]
$Rb_4Sn_3Cl_2Br_8$	$Cmc2_1$	2.82	0.084[19]	0.5	[25]
$Cs_2SnCl_2I_2$	*I4/mmm*	2.62	0.166[19]	/	[26]
$Rb_3SnCl_3I_2$	*Pnma*	2.53	0.127[19]	/	[26]
$Cs_2Sn_6F_{11}Br_3$	*C2/m*	/	/	/	[27]
$Rb_6Sn_5F_{10}I_6$	*C2/m*	2.10	0.119[19]	/	[28]
$Cs_8Sn_6Br_{13}I_7$	*Cmcm*	/	/	/	[29]

2. Results and Discussion

2.1. Structures of $Rb_2Sn_2F_5Cl$ and $Cs_2Sn_2F_5Cl$

Compounds $Rb_2Sn_2F_5Cl$ and $Cs_2Sn_2F_5Cl$ are isostructural and crystallize in the space group *Pnma* (No. 62). Hence, only the structure of $Rb_2Sn_2F_5Cl$ will be discussed in detail (Figure 1). The unit cell of $Rb_2Sn_2F_5Cl$ is illustrated in Figure S1 (Supporting Information). In the asymmetric unit, Rb, Sn, F, and Cl occupy two, two, three, and one crystallographically unique positions, respectively (Table S1, Supporting Information). As shown in Figure S2 (Supporting Information), each Sn atom is coordinated with three F atoms and one Cl atom to form $[SnF_3Cl]^{2-}$ group. Despite that $[SnF_3Cl]^{2-}$ unit once emerged in the compound SnClF,[31] this is the first time $[SnF_3Cl]^{2-}$ appears in the metal Sn^{2+}-based halides. Attributable to the stereochemically active lone pair on Sn^{2+}, the ligands F and Cl atoms are pushed to one side of Sn atom. Then, $[Sn(1)F_3Cl]^{2-}$ and $[Sn(2)F_3Cl]^{2-}$ groups share one common F atom to form a $[Sn_2F_5Cl_2]^{3-}$ dimer, which further

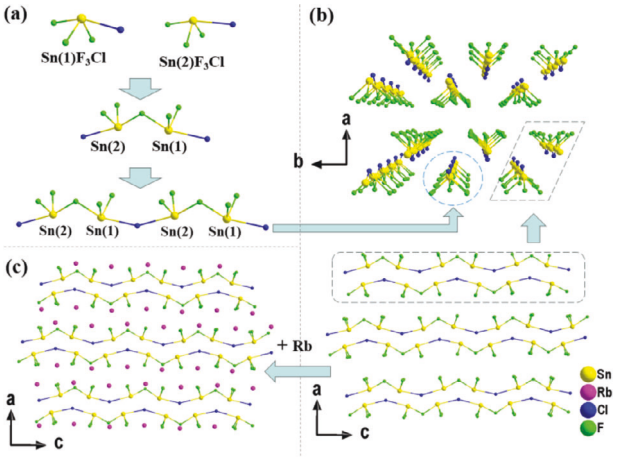

Figure 1. The crystal structure of $Rb_2Sn_2F_5Cl$. a) The $[Sn_2F_5Cl_2]^{3-}$ dimer and a 1D $[Sn_2F_5Cl]_\infty$ chain. b) The arrangement of $[Sn_2F_5Cl]_\infty$ chains. c) Crystallographic structure of $Rb_2Sn_2F_5Cl$ along b-axis.

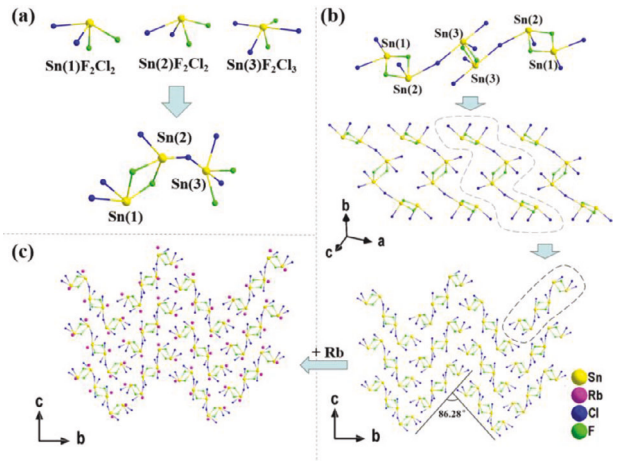

Figure 2. The crystal structure of $RbSnFCl_2$. a) The $[Sn_3F_4Cl_6]^{4-}$ cluster. b) The arrangement of isolated $[Sn_6F_6Cl_{12}]^{6-}$ short chains. c) Crystallographic structure of $RbSnFCl_2$ along a-axis.

constitute the 1D $[Sn_2F_5Cl]_\infty$ chain along the c-axis via sharing the common Cl atoms (Figure 1a). As shown in Figure 1b, the $[Sn_2F_5Cl]_\infty$ chains are stacked along a-axis in an antiparallel manner, that results in the cancellation of individual microscopic polarizability and dipole moments. However, the chained structure with lone pairs still presents a strong anisotropy, which is reflected in the rod-like morphology of the obtained crystals of $Rb_2Sn_2F_5Cl$ and $Cs_2Sn_2F_5Cl$ (Figure S3, Supporting Information). The two kinds of Rb^+ cations are in the interstices between $[Sn_2F_5Cl]_\infty$ chains to balance the charge (Figure 1c).

As shown in Figure S2 (Supporting Information), Rb(1) is in tenfold coordination with nine F and one Cl atoms, and Rb(2) is bonded to six F and two Cl atoms. The Rb-F and Rb-Cl bond distances are in the ranges of 2.859(3)–3.433(4) Å and 3.410(3)–3.796(2) Å, respectively. The Sn—F and Sn—Cl bond distances change in the ranges of 2.008(3)–2.280(4) Å and 2.824(2)–2.999(2) Å, respectively (Table S2, Supporting Information). Bond valence calculations[32] on Rb, Sn, F, and Cl resulted in values of 0.90–1.08, 2.26–2.28, 1.06–1.22, and 0.68, respectively (Table S1, Supporting Information). These values are consistent with the reported oxidation states.[25,33]

2.2. Structures of $RbSnFCl_2$ and $CsSnFCl_2$

Compounds $RbSnFCl_2$ and $CsSnFCl_2$ have similar structures and crystallize into a monoclinic crystal system with a centric space group of $P2_1/n$ (No. 14). The unit cell of $RbSnFCl_2$ and $CsSnFCl_2$ are illustrated in Figure S4 (Supporting Information). For $RbSnFCl_2$, there are three Rb atoms, three Sn atoms, three F atoms, and six Cl atoms in its asymmetric unit (Table S3, Supporting Information). As shown in Figure 2a, The Sn atoms in this structure have three coordination patterns: Sn(1) and Sn(2) are coordinated with two F^- anions and two Cl^- atoms to form $[SnF_2Cl_2]^{2-}$ polyhedra, respectively, Sn(3) is coordinated with two F^- anions and three Cl^- anions to form a novel $[SnF_2Cl_3]^{3-}$ group. One $[Sn(1)F_2Cl_2]^{2-}$ polyhedron and one $[Sn(2)F_2Cl_2]^{2-}$ polyhedron further build a $[Sn_2F_2Cl_4]^{2-}$ dimer by sharing their common edge, and the $[Sn_2F_2Cl_4]^{2-}$ dimer and $[Sn(3)F_2Cl_3]^{3-}$ polyhedron connect with each other by sharing Cl atom to form the $[Sn_3F_4Cl_6]^{4-}$ cluster. As shown in Figure 2b, two $[Sn_3F_4Cl_6]^{4-}$ clusters are further connected by sharing the F atoms to form a $[Sn_6F_6Cl_{12}]^{6-}$ short chain. In the structure, the $[Sn_6F_6Cl_{12}]^{6-}$ short chains are arranged along the a-axis direction. Interestingly, on the b–c plane, the two adjacent $[Sn_6F_6Cl_{12}]^{6-}$ short chains have an angle of 86.28°, exhibiting a wavy structure. As shown in Figure 2c, the Rb^{2+} cations are in the interstices of the $[Sn_6F_6Cl_{12}]^{6-}$ short chains to balance the charge.

As shown in Figure S5 (Supporting Information), Rb atoms are coordinated with two F and eight Cl atoms. The Rb-F and Rb-Cl bond distances are in the ranges of 2.845(6)–2.967(5) Å and 3.275(3)–3.863(3) Å, respectively. The Sn—F bonds change from 2.085(5) to 2.358(7) Å, and Sn—Cl bonds range from 2.491(5) to 2.820(5) Å (Table S4, Supporting Information). Bond valence calculations on Rb, Sn, F, and Cl resulted in values of 0.99–1.03, 1.70–1.85, 0.96–1.15, and 0.64–1.07, respectively (Table S3, Supporting Information). These values are consistent with the reported oxidation states.[25,33]

2.3. Structural Comparison

Title compounds $Rb_2Sn_2F_5Cl$ and $RbSnFCl_2$ can be obtained through partial substitution of F atom with Cl atom in the compound $RbSnF_3$[34] (Figure 3).

The structural evolution from $RbSnF_3$ to $Rb_2Sn_2F_5Cl$ will be discussed in detail. $RbSnF_3$ and $Rb_2Sn_2F_5Cl$ feature similar 1D chain structure formed by FBB $[SnX_4]^{2-}$ (X = halogen) polyhedra. In $RbSnF_3$, the $[Sn_2F_6]_\infty$ chain is built by the FBB $[SnF_4]^{2-}$ units; in $Rb_2Sn_2F_5Cl$, the FBB is changed to $[SnF_3Cl]^{2-}$ from $[SnF_4]^{2-}$ polyhedron after one F atom replaced with one Cl atom (Figure S6, Supporting Information). Considering that the Cl atom has a much larger ionic radius compared with the F atom (Table S5, Supporting Information), the structural distortion is enhanced from $[SnF_4]^{2-}$ to $[SnF_3Cl]^{2-}$, and Sn—X bond lengths change from 1.987–2.518 to 2.009–2.999 Å, respectively. As shown in the shaded area in Figure S6 (Supporting Information), the 1D $[Sn_2F_6]_\infty$ chains in $RbSnF_3$ have four different orientations, while the $[Sn_2F_5Cl]_\infty$ chains in $Rb_2Sn_2F_5Cl$ have only two orientations, more approaching ideal arrangement mode. Hence, the newly generated $[SnF_nX_m]$ group can help to regulate the spatial arrangement of the building blocks. In Figure S6 (Supporting Information), all the compounds feature 1D $[Sn—X]_\infty$ chains, but these 1D chains are not arranged in an ideal mode. We speculate that, the introduction of large-size halogen atoms (Br and I)

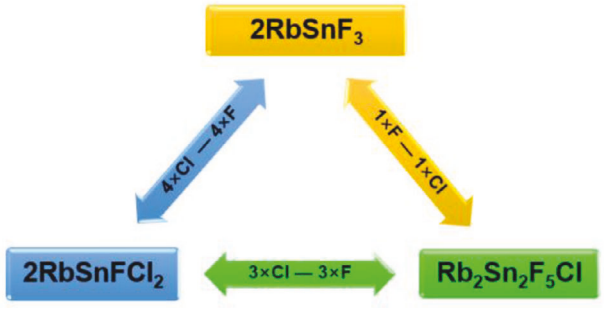

Figure 3. The evolution of $Rb_2Sn_2F_5Cl$, $RbSnFCl_2$, and $RbSnF_3$.

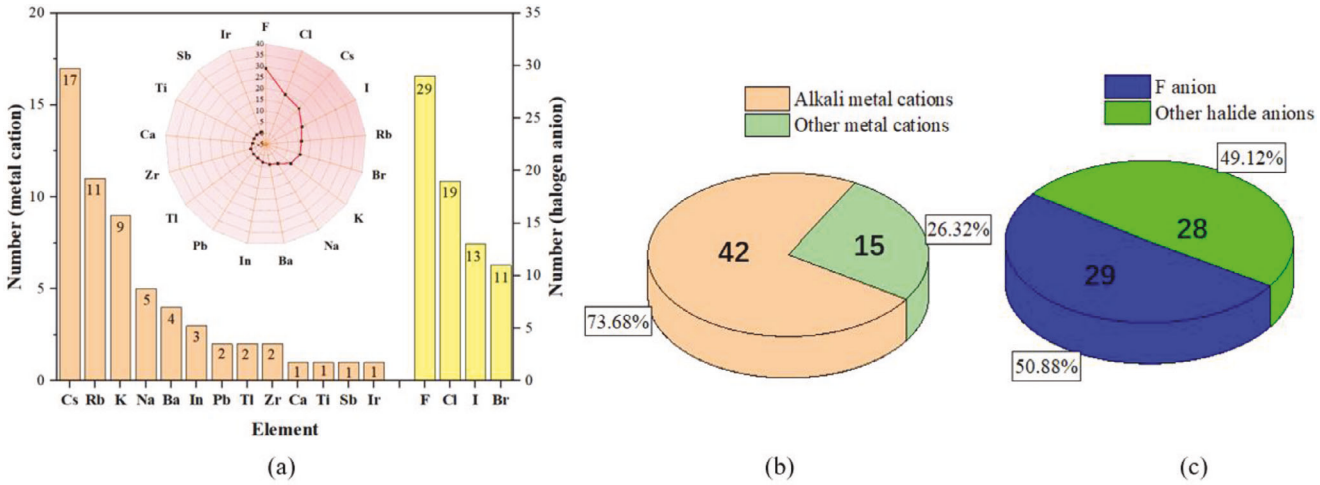

Figure 4. a) The number of Sn^{2+} halides containing different elements, b) the proportion of alkali metal Sn^{2+} halides, and c) the proportion of Sn^{2+} fluorides.

may further optimize the chains arrangement and promote the generation of excellent birefringent crystals.

2.4. Structural Chemistry of Metal Sn^{2+}-Based Halides

The diverse coordination modes and spatial configurations of [Sn—X] units drive us to further explore their structural chemistry. According to the investigation in the recent publications and inorganic crystal structure database (ICSD version 5.1.0, the last release of ICSD-2023.2), there are 57 compounds in the family of metal Sn^{2+}-based halides (Tables S6–S9, Supporting Information).

In the metal Sn^{2+} halides system, the frequency of occurrence of the related elements as chemical constituents is shown in Figure 4. Obviously, there are nearly 74% of compounds containing alkali metal elements. And more than half of the metal Sn halides contain F element. Alkali metal cations are free of d–d or f–f electronic transitions, and the are beneficial for good transparency in the UV spectral region. Owing to the largest electronegativity, F atom can also shift the cutoff edge to the shorter wavelength region. In addition, halide compounds always own the wider IR transparent window compared with oxides. Based on the above analysis, it is speculated that the alkali metal Sn-based halide system may be conducive to explore optical crystals with wide transparent range from UV to IR region.

Tables S6–S9 (Supporting Information) show the distribution of [Sn—X] anionic frameworks with different dimensions in metal Sn halides. Metal Sn halides can be divided into four categories according to their specific dimensions (Figure 5): 0D isolated clusters (24.56%), 1D infinite chains (17.54%), 2D infinite layers (43.86%), and 3D networks (14.04%).

SCALP cation Sn^{2+} has received a great deal of research attention for its multiple coordination modes. In metal Sn halides, Sn^{2+} has been observed in three-, four-, five-, six-, and seven-coordination environments. There are 26 types of Sn-centered polyhedra found in this family (Figure 6; Table S10, Supporting Information), among which $[SnF_3Cl]^{2-}$ and $[SnF_2Cl_3]^{3-}$ dis-

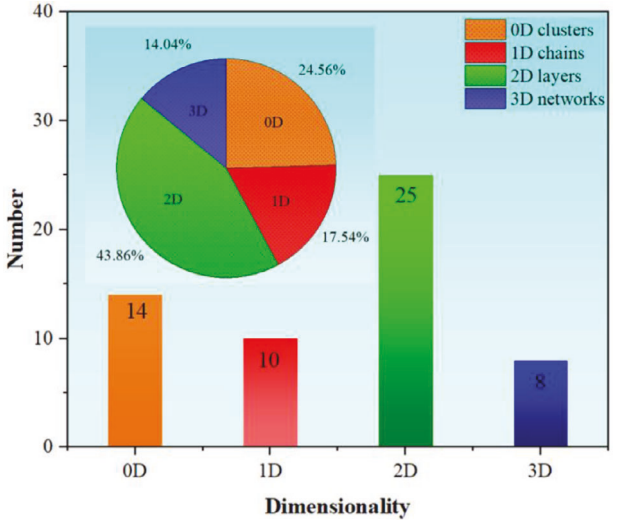

Figure 5. Frequency of occurrence metal Sn halides with different dimensions. Inset: corresponding proportion in percentage (%).

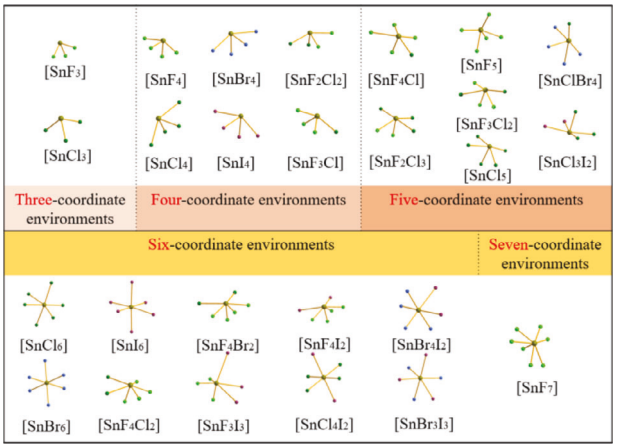

Figure 6. [Sn—X] polyhedra with different coordination environments.

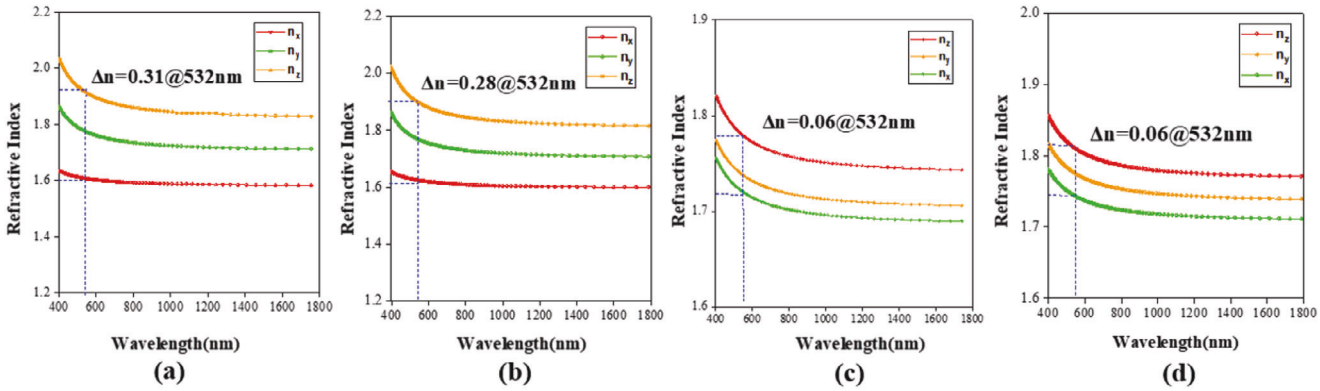

Figure 7. The calculated refractive index and birefringence curves of a) $Rb_2Sn_2F_5Cl$, b) $Cs_2Sn_2F_5Cl$, c) $RbSnFCl_2$, and d) $CsSnFCl_2$.

torted polyhedra are first discovered in metal Sn^{2+}-based halide family.

After structural comparisons, we found that the dimension of [Sn-X] framework in metal Sn^{2+}-based halides is affected by the following factors:

(a) The atomic percentage of Sn. The smaller atomic percentage of Sn means that there are fewer Sn atoms per unit cell. As shown in Table S11 (Supporting Information), when the atomic percentage of Sn is smaller than 0.2, most compounds feature isolated [Sn—X] clusters.

(b) The bond length of [Sn—X] FBB. From Table S11 (Supporting Information), it is also found that Sn-based halides with 3D networks do not contain F element. This phenomenon may be attributed to that F element with smaller atomic radius is more likely to form shorter Sn—F bond compared with Sn—Cl/Br/I bond, so the compounds containing shorter Sn—X bonds tend to form low-dimensional frameworks.

(c) The coordination modes of Sn. In general, the Sn atom with more coordinated atoms is easier to connect with each other to form the high-dimensional $[Sn—X]_\infty$ framework. Compounds containing $[SnX_3]$ FBB are more likely to form 0D structures (like $CsSnF_3$), while compounds containing $[SnX_6]$ FBB are more likely to form 3D structures (like $Rb_4Sn_3Cl_2Br_8$).

(d) The influence of lone pair electrons on Sn^{2+}. Due to the repulsive force between the lone pair electrons and the bonding electrons of Sn^{2+} atom, the ligands are all pushed toward one side of the Sn^{2+} cation (Table S11, Supporting Information). Therefore, different [Sn—X] groups are difficult to link together to construct complex high-dimensional frameworks due to the repulsion of lone pairs. Seen from Table S11 (Supporting Information), the lone pairs of $[SnX_6]$ units (X = Br and/or I) seem stereochemically inactive. Therefore, without the repulsion of lone pairs, compounds $Rb_4Sn_3Cl_2Br_8$, $CsSnI_3$, $CsSnBr_3$, $Cs_2SnCl_2I_2$, and $Cs_8Sn_6Br_{13}I_7$ (listed in Table S11, Supporting Information) built by $[SnX_6]$ FBBs, display complex 3D network structure.

Through the comprehensive analyses on crystal structures and structure–property relationship of metal Sn^{2+}-based halide family, we believe our work and insights will facilitate the further exploration of metal Sn^{2+}-based halide system.

2.5. Optical Properties

The UV–vis–NIR diffuse reflectance spectra of title compounds were tested using the pure samples (Figure S7, Supporting Information). $A_2Sn_2F_5Cl$ and $ASnFCl_2$ (A = Rb, Cs) exhibit short UV cutoff edges at about 280, 287, 302, and 306 nm, corresponding to the bandgaps of 4.43, 4.32, 4.11, and 4.05 eV, respectively, which indicate that they may possess high laser damage threshold (LDTs; Figure S8, Supporting Information). The IR spectra of $A_2Sn_2F_5Cl$ and $ASnFCl_2$ were deposited in Figure S9 (Supporting Information). The peaks around 560, 554, 487, 474, and 432 cm^{-1} can be attributed to Sn—F stretches.[35] And it is obviously shown that there is no absorption peak from 4000 to 600 cm^{-1}, corresponding a wide IR transparent window up to 16.6 μm, which is superior to most oxide compounds.

Therefore, the title compounds have wide transparent range from UV to IR region, which covers two important mid-IR atmospheric windows of 3–5 μm and 8–12 μm. Thus, $A_2Sn_2F_5Cl$ and $ASnFCl_2$ can be potentially used in the UV–vis–IR region.

2.6. Thermal Behavior

As shown in Figure S10 (Supporting Information), it exhibits the TG–DSC curves of compounds $Rb_2Sn_2F_5Cl$, $Cs_2Sn_2F_5Cl$, and $RbSnFCl_2$. It was observed that the decomposition temperatures for $Rb_2Sn_2F_5Cl$, $Cs_2Sn_2F_5Cl$, and $RbSnFCl_2$ are approximately 251, 236, and 200 °C, respectively. The TG curves show that the weight losses for compounds $Rb_2Sn_2F_5Cl$, $Cs_2Sn_2F_5Cl$, and $RbSnFCl_2$ are about 10%, 16%, and 40% during the heating process respectively. Figure S11 (Supporting Information) shows the powder XRD patterns of final residuals after melting. For $Rb_2Sn_2F_5Cl$ and $Cs_2Sn_2F_5Cl$, the final residuals are ACl (A = Rb, Cs) and SnFCl. For $RbSnFCl_2$ and $CsSnFCl_2$, the residues are ACl (A = Rb, Cs) and SnO. The thermal behaviors of the decomposition products are consistent with those reported previously.[23]

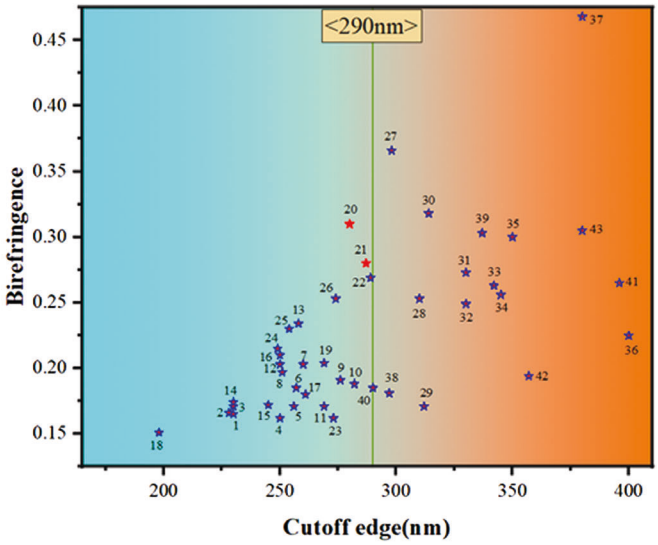

1	$Na_3Rb_6(CO_3)_3(NO_3)_2Br{\cdot}6H_2O$	12	$SrI_2O_5F_2$	23	$KGd(CO_3)_2$	34	$CdTeMoO_6$
2	$Na_3Rb_6(CO_3)_3(NO_3)_2Cl{\cdot}6H_2O$	13	$Sn(IO)_2F_2$	24	$KTb(CO_3)_2$	35	$NaNO_2$
3	$CaCO_3$	14	$BaI_2O_5F_2$	25	$LiGa(IO_3)_4$	36	YVO_4
4	$K_2Sb(P_2O_7)F$	15	$Be_2(BO_3)(IO_3)$	26	β-$Sc(IO_3)_3$	37	Sn_2PO_4I
5	$Gd(OH)_2NO_3$	16	$Na_3Cs(MoO_2F_4)_2$	27	$Sc(IO_3)_2(NO_3)$	38	Sn_2PO_4Cl
6	$Y(OH)_2NO_3$	17	$SbHPO_3F$	28	$[Al(H_2O)_6](IO_3)_2(NO_3)$	39	Sn_2PO_4Br
7	$La(OH)_2NO_3$	18	$Ba_3Sc_2(BO_3)_4$	29	$Sn_2B_5O_9Cl$	40	$BaTi(BO_3)_2$
8	$NaGaI_3O_9F$	19	$Rb[SnF(HPO_4)]$	30	SbB_3O_6	41	$Sn_{14}O_{11}Br_6$
9	α-SnF_2	20	$Rb_2Sn_2F_5Cl$	31	$Sn_2B_5O_9Br$	42	$LiNa_5Mo_9O_{30}$
10	$[In(IO_3)(OH)(H_2O)](NO_3)$	21	$Cs_2Sn_2F_5Cl$	32	$NaNO_3$	43	α-$BaTeMo_2O_9$
11	$NaZnCO_3F$	22	$NaPb_2(CO_3)_2F$	33	$RbTeMo_2O_8F$		

Figure 8. A summary of inorganic compounds with birefringence larger than 0.15 and UV cutoff edge shorter than 400 nm (only some representative compounds are listed in 290–400 nm). 1, $Na_3Rb_6(CO_3)_3(NO_3)_2Br{\cdot}6H_2O$; 2, $Na_3Rb_6(CO_3)_3(NO_3)_2Cl{\cdot}6H_2O$; 3, $CaCO_3$; 4, $K_2Sb(P_2O_7)F$; 5, $Gd(OH)_2NO_3$; 6, $Y(OH)_2NO_3$; 7, $La(OH)_2NO_3$; 8, $NaGaI_3O_9F$; 9, α-SnF_2; 10, $[In(IO_3)(OH)(H_2O)](NO_3)$; 11, $NaZnCO_3F$; 12, $SrI_2O_5F_2$; 13, $Sn(IO)_2F_2$; 14, $BaI_2O_5F_2$; 15, $Be_2(BO_3)(IO_3)$; 16, $Na_3Cs(MoO_2F_4)_2$; 17, $SbHPO_3F$; 18, $Ba_3Sc_2(BO_3)_4$; 19, $Rb[SnF(HPO_4)]$; 20, $Rb_2Sn_2F_5Cl$; 21, $Cs_2Sn_2F_5Cl$; 22, $NaPb_2(CO_3)_2F$; 23, $KGd(CO_3)_2$; 24, $KTb(CO_3)_2$; 25, $LiGa(IO_3)_4$; 26, β-$Sc(IO_3)_3$; 27, $Sc(IO_3)_2(NO_3)$; 28, $[Al(H_2O)_6](IO_3)_2(NO_3)$; 29, $Sn_2B_5O_9Cl$; 30, SbB_3O_6; 31, $Sn_2B_5O_9Br$; 32, $NaNO_3$; 33, $RbTeMo_2O_8F$; 34, $CdTeMoO_6$; 35, $NaNO_2$; 36, YVO_4; 37, Sn_2PO_4I; 38, Sn_2PO_4Cl; 39, Sn_2PO_4Br; 40, $BaTi(BO_3)_2$; 41, $Sn_{14}O_{11}Br_6$; 42, $LiNa_5Mo_9O_{30}$; 43, α-$BaTeMo_2O_9$.

2.7. Theoretical Calculations

To further understand the relationship between the electronic structure and optical properties of $Rb_2Sn_2F_5Cl$, $Cs_2Sn_2F_5Cl$, $RbSnFCl_2$, and $CsSnFCl_2$, theoretical calculation was performed based on DFT. The calculated band structure (Figure S12, Supporting Information) shows that compounds $Rb_2Sn_2F_5Cl$, $Cs_2Sn_2F_5Cl$, and $CsSnFCl_2$ are direct bandgap compounds, whereas $RbSnFCl_2$ is an indirect bandgap compound. The GGA-PBE bandgaps of $Rb_2Sn_2F_5Cl$, $Cs_2Sn_2F_5Cl$, $RbSnFCl_2$, and $CsSnFCl_2$ are 2.83, 2.89, 2.82, and 2.83 eV, respectively, which are smaller than the measured values because of the discontinuity of the exchange-correlation energy in DFT calculations.[36]

To understand the composition and origination of the electronic structures, the total density of states (TDOS) and projected density of states (PDOS) were obtained (Figure S13, Supporting Information). Because the title compounds are structural similar, the band structures of the $Rb_2Sn_2F_5Cl$ and $RbSnFCl_2$ were described in detail for representation. As shown in Figure S13a (Supporting Information), the states from −5 eV to the Fermi

level for compound $Rb_2Sn_2F_5Cl$ are primarily composed of Cl-3p, F-2p, Sn-5p, and Sn-5s orbitals. The conduction band between 0 and 5 eV consists of Sn-5s and Sn-5p orbitals. In the same way, Figure S13c (Supporting Information) shows that the states of $RbSnFCl_2$ from −5 eV to the Fermi level mostly consist of Cl-3p, F-2p, Sn-5p, and Sn-5s orbitals, and the conduction band of 0–5 eV is mainly ascribed to the Sn-5s and Sn-5p states. The PDOS of the four compounds shows that Sn-5s and Sn-5p orbitals overlap with Cl-3p and F-2p orbitals, indicating a strong interaction between Sn, F, and Cl atoms. It is well known that the electronic transition from the valance band maximum (VBM) to the conduction band minimum (CBM) near the Fermi level determines the optical performance of optical materials. Thus, the theoretical studies suggest that the liner optical properties of the four title compounds are mainly derived from the Sn-centered distorted polyhedra.

The calculated refractive index curves of title compounds were shown in Figure 7. The birefringences are ≈0.06 for $RbSnFCl_2$ and $CsSnFCl_2$ at 532 nm. Significantly, $Rb_2Sn_2F_5Cl$ and $Cs_2Sn_2F_5Cl$ exhibit the largest birefringence in current reported Sn-based halides, and the birefringences are 0.31 and 0.28 at 532 nm, respectively (Table S12, Figure S14, Supporting Information). Figure 8 also illustrates that $A_2Sn_2F_5Cl$ have the largest birefringence among inorganic birefringent crystals with UV cutoff edges lower than 290 nm (Table S13, Supporting Information). Taking above spectra analyses into consideration, $A_2Sn_2F_5Cl$ have better-balanced optical properties of sufficiently large birefringence (≈0.30 at 532 nm), short UV cutoff edge (≈280 nm) and wide transparent range (0.28–16.6 μm), so they probably become the alternative candidates for optical applications in the UV–IR region.

Electron Localization Function (ELF) analyses for these four compounds were also conducted to visualize the interatomic interactions. As shown in Figure S15 (Supporting Information), it is observed that the map clearly reveals the asymmetric lobe on Sn^{2+}, which stems from the polar nature of the Sn and results in the large birefringence.[37] To further prove this influence, the dipole moments of cationic polyhedra for these compounds were calculated and the results were listed in Table S14 (Supporting Information).[38] The magnitude of the dipole moment of Sn-centered polyhedra are much higher than that of alkali metal-centered polyhedra. For example, in $Rb_2Sn_2F_5Cl$, the calculated values of $[SnF_3Cl]$ (16.3 D and 17.4 D) are several times higher than the values of $[RbF_9Cl]$ (2.17 D) and $[RbF_6Cl_2]$ (4.99 D). Therefore, the large birefringence of title compounds could be ascribed to the synergistic effect of Sn^{2+} lone pair cations and mixed halogen anions, while the role of alkali metal cations is reflected in widening the optical bandgaps.

3. Conclusion

In summary, four new Sn^{2+}-based halides $A_2Sn_2F_5Cl$ and $ASnFCl_2$ (A = Rb, Cs) have been synthesized successfully by the hydrothermal method. And their crystal structures and optical properties are discussed in detail. Especially, $A_2Sn_2F_5Cl$ (A = Rb, Cs) exhibit the largest birefringences (0.31 and 0.28 at 532 nm) among all the reported Sn-based halides, and the outstanding birefringence stems from the distorted Sn-centered polyhedra. Besides, $A_2Sn_2F_5Cl$ show short UV cutoff edges (≈280 nm, corresponding large LDTs) and wide transparent region (0.28–16.6 μm). These advantages indicate that $A_2Sn_2F_5Cl$ have well-balanced optical properties, which make them become prospective birefringent crystals in UV–vis–IR region. Therefore, this work provides a synthetic strategy to achieve the coexistence of unparalleled birefringence, large bandgap and wide transparent region, and this will help to find new birefringence crystal materials with good comprehensive performance. In addition, we also have made a comprehensive analysis on crystal structures and structure–property relationship of metal Sn^{2+}-based halide family, which will facilitate the further exploration of this system.

Supporting Information

Supporting Information is available from the Wiley Online Library or from the author.

Acknowledgements

This work was supported by Shanghai Institute of Technology (10120K238005-A06, 1021GK230003056-B20), the National Natural Science Foundation of China (grant nos. 52072109), the Welch Foundation (grant E-1457), the NSF (DMR-2002319) and the Science and Technology Project of Hebei Education Department (grant no. BJK2023029).

Conflict of Interest

The authors declare no conflict of interest.

Data Availability Statement

The data that support the findings of this study are available in the supplementary material of this article.

Keywords

birefringent materials, mixed halogen ions, optical anisotropy, SCALP cations

Received: October 6, 2023
Revised: November 11, 2023
Published online: December 15, 2023

[1] a) G. Ghosh, *Opt. Commun.* **1999**, *163*, 95; b) J. Hecht, *Appl. Opt.* **2010**, *49*, 99; c) R. Li, Z. Krist, *Cryst. Mater.* **2013**, *228*, 526.
[2] a) G. Zhou, J. Xu, X. Chen, H. Zhong, F. Gan, *J. Cryst. Growth* **1998**, *191*, 517; b) Z. Xie, L. Sun, G. Han, Z. Gu, *Adv. Mater.* **2008**, *20*, 3601; c) M. F. Weber, C. A. Stover, L. R. Gilbert, T. J. Nevitt, A. J. Ouderkirk, *Science* **2000**, *287*, 2451; d) J. Min, A. Abudurusuli, J. Li, S. Pan, Z. Yang, *Phys. Chem. Chem. Phys.* **2020**, *22*, 19697; e) P. Hlubina, D. Ciprian, L. Knyblová, *Opt. Commun.* **2006**, *260*, 535.
[3] H. Luo, T. Tkaczyk, E. L. Dereniak, K. Oka, R. Sampson, *Opt. Lett.* **2006**, *31*, 616.
[4] F. Sedlmeir, R. Zeltner, G. Leuchs, H. G. L. Schwefel, *Opt. Express* **2014**, *22*, 30934.
[5] a) D. L. DeShazer, *J. Lightwave Technol.* **2002**, *4481*, 10; b) S. Niu, G. Joe, H. Zhao, Y. Zhou, T. Orvis, H. Huyan, J. Salman, K. Mahalingam, B. Urwin, J. Wu, Y. Liu, T. E. Tiwald, S. B. Cronin, B. M. Howe, M. Mecklenburg, R. Haiges, D. J. Singh, H. Wang, M. A. Kats, J. Ravichandran, *Nat. Photonics* **2018**, *12*, 392.

[6] C. Wu, T. Wu, X. Jiang, Z. Wang, H. Sha, L. Lin, Z. Lin, Z. Huang, X. Long, M. G. Humphrey, C. Zhang, *J. Am. Chem. Soc.* **2021**, *143*, 4138.
[7] a) X. Chen, B. Zhang, F. Zhang, Y. Wang, M. Zhang, Z. Yang, K. R. Poeppelmeier, S. Pan, *J. Am. Chem. Soc.* **2018**, *140*, 16311; b) J. Lu, Y. Lian, L. Xiong, Q. Wu, M. Zhao, K. Shi, L. Chen, L. Wu, *J. Am. Chem. Soc.* **2019**, *141*, 16151; c) Z. Hu, L. Liu, R. Zhang, Q. Jing, H. Wang, J. Tian, J. Xu, P. S. Halasyamani, *J. Mater. Chem. C* **2023**, *11*, 3325; d) H. Liu, Y. Wang, B. Zhang, Z. Yang, S. Pan, *Chem. Sci.* **2020**, *11*, 694.
[8] a) D. Lin, M. Luo, C. Lin, F. Xu, N. Ye, *J. Am. Chem. Soc.* **2019**, *141*, 3390; b) Y. Li, X. Zhang, J. Zheng, Y. Zhou, W. Huang, Y. Song, H. Wang, X. Song, J. Luo, S. Zhao, *Angew. Chem., Int. Ed.* **2023**, *62*, e202304498; c) Y. Xu, C. Lin, D. Lin, M. Luo, D. Zhao, L. Cao, N. Ye, *Inorg. Chem.* **2020**, *59*, 15962; d) Q. Xu, W. Huang, H. Wang, Y. Li, Y. Zhou, L. Hou, S. Zhao, J. Luo, *Small* **2023**, 2304333.
[9] X. Liu, L. Kang, P. Gong, Z. Lin, *Angew. Chem., Int. Ed.* **2021**, *60*, 13574.
[10] C. Wu, X. Jiang, Z. Wang, L. Lin, Z. Lin, Z. Huang, X. Long, M. G. Humphrey, C. Zhang, *Angew. Chem., Int. Ed.* **2021**, *60*, 3464.
[11] a) Y. Yang, Y. Qiu, P. Gong, L. Kang, G. Song, X. Liu, J. Sun, Z. Lin, *Chem. Eur. J.* **2019**, *25*, 5648; b) X. Zhang, B. Yang, J. Chen, C. Hu, Z. Fang, Z. Wang, J. Mao, *Chem. Commun.* **2020**, *56*, 635; c) J. Guo, A. Tudi, S. Han, Z. Yang, S. Pan, *Angew. Chem., Int. Ed.* **2021**, *60*, 24901; d) Z. Lu, F. Zhang, A. Tudi, Z. Yang, Z. Li, S. Pan, *J. Mater. Chem. C* **2021**, *9*, 7103; e) X. Lu, Z. Chen, X. Shi, Q. Jing, M. H. Lee, *Angew. Chem., Int. Ed.* **2020**, *59*, 17648.
[12] H. Wang, L. Liu, Z. Hu, J. Wang, M. Zhu, Y. Meng, J. Xu, *Inorg. Chem.* **2023**, *62*, 557.
[13] a) Z. Bai, J. Lee, H. Kim, Y. Kuk, M. H. Choi, C. Hu, K. M. Ok, *Small* **2023**, *19*, e2207709; b) N. Ma, J. Chen, B. Li, C. Hu, J. Mao, *Small* **2023**, 2304388.
[14] Y. Liu, X. Liu, S. Liu, Q. Ding, Y. Li, L. Li, S. Zhao, Z. Lin, J. Luo, M. Hong, *Angew. Chem., Int. Ed.* **2020**, *59*, 7793.
[15] a) X. Chen, H. Jo, K. M. Ok, *Angew. Chem., Int. Ed.* **2020**, *59*, 7514; b) X. Chen, K. M. Ok, *Chem. Sci.* **2022**, *13*, 3942; c) X. Chen, Q. Jing, K. M. Ok, *Angew. Chem., Int. Ed.* **2020**, *59*, 20323; d) P. Gong, F. Liang, L. Kang, X. Chen, J. Qin, Y. Wu, Z. Lin, *Coordin. Chem. Rev.* **2019**, *380*, 83.
[16] a) C. C. Stoumpos, C. D. Malliakas, M. G. Kanatzidis, *Inorg. Chem.* **2013**, *52*, 9019; b) Y. You, W. Liao, D. Zhao, H. Ye, Y. Zhang, Q. Zhou, X. Niu, J. Wang, P. Li, D. Fu, Z. Wang, S. Gao, K. Yang, J. Liu, J. Li, Y. Yan, R. Xiong, *Science* **2017**, *357*, 306.
[17] J. Guo, A. Tudi, S. Han, Z. Yang, S. Pan, *Angew. Chem., Int. Ed.* **2021**, *60*, 3540.
[18] T. Liu, G. Qin, G. Zhang, T. Zhu, F. Niu, Y. Wu, C. Chen, *Appl. Phys. Lett.* **2008**, *93*, 091.
[19] J. Guo, J. Huang, A. Tudi, X. Hou, S. Han, Z. Yang, S. Pan, *Angew. Chem., Int. Ed.* **2023**, *62*, e202340638.
[20] G. Zhang, J. Qin, T. Liu, T. Zhu, P. Fu, Y. Wu, C. Chen, *Cryst. Growth Des.* **2008**, *8*, 2946.
[21] a) G. Zhang, Y. Li, K. Jiang, H. Zeng, C. Chen, *J. Am. Chem. Soc.* **2012**, *134*, 14818; b) Q. Wu, X. Meng, C. Zhong, X. Chen, J. Qin, *J. Am. Chem. Soc.* **2014**, *136*, 5683.
[22] Z. Setifi, H. Merazig, P. H. Bird, F. Setifi, K. Tam, G. Dénès, *Acta Crystallogr., Sect. E: Struct. Rep. Online* **2005**, *61*, 120.
[23] P. Gong, S. Luo, Q. Huang, Y. Yang, X. Jiang, F. Liang, C. Chen, Z. Lin, *J. Solid State Chem.* **2017**, *248*, 104.
[24] P. Gong, S. Luo, K. Xiao, Q. Huang, Y. Yang, H. Huang, Y. Wu, C. Chen, Z. Lin, *Inorg. Chem.* **2017**, *56*, 3081.
[25] P. Gong, S. Luo, Y. Yang, F. Liang, S. Zhang, S. Zhao, J. Luo, Z. Lin, *Cryst. Growth Des.* **2018**, *18*, 380.
[26] J. Li, C. C. Stoumpos, G. G. Trimarchi, I. Chung, L. Mao, M. Chen, M. R. Wasielewski, L. Wang, M. G. Kanatzidis, *Chem. Mater.* **2018**, *30*, 4847.
[27] I. Abrahams, J. D. Donaldson, S. M. Grimes, *J. Chem. Soc. Dalton Trans.* **1992**, *23*, 669.
[28] C. C. Stourripos, L. Mao, C. D. Malliakas, M. G. Kanatzidis, *Inorg. Chem.* **2017**, *56*, 56.
[29] O. Nazarenko, M. R. Kotyrba, S. Yakunin, M. Wörle, B. M. Benin, G. Rainò, F. Krumeich, M. Kepenekian, J. Even, C. Katan, M. V. Kovalenko, *Chem. Mater.* **2019**, *31*, 2121.
[30] a) Y. Shen, L. Huang, Z. Wang, Y. Zhou, X. Xue, H. Lin, R. Yan, S. Zhao, J. Luo, *Inorg. Chem.* **2022**, *61*, 4468; b) R. Li, Y. Ma, *Cryst. Eng. Commun.* **2012**, *14*, 5421; c) Y. Wu, T. Sasaki, S. Nakai, A. Yokotani, H. Tang, C. Chen, *Appl. Phys. Lett.* **1993**, *62*, 2614; d) Y. Mori, I. Kuroda, S. Nakajima, A. Taguchi, T. Sasaki, S. Nakai, *J. Cryst. Growth* **1995**, *156*, 307.
[31] C. Geneys, S. Vilminot, L. Cot, *Acta Crystallogr., Sect. B: Struct. Crystallogr. Cryst. Chem.* **1976**, *32*, 3199.
[32] a) N. E. Brese, M. O'keeffe, *Acta Crystallogr. B.* **1991**, *47*, 192; b) I. D. Brown, D. Altermatt, *Acta Crystallogr. B.* **1985**, *41*, 244.
[33] a) M. Ji, C. Hu, Z. Fang, Y. Chen, J. Mao, *Inorg. Chem.* **2021**, *60*, 15744; b) Z. Lin, P. Gong, Y. Yang, S. Luo, F. Liang, X. Jiang, *Inorg. Chem.* **2017**, *56*, 13593.
[34] T. Thao Tran, P. Shiv Halasyamani, *J. Solid State Chem.* **2014**, *210*, 213.
[35] R. H. Hauge, J. W. Hastie, J. L. Margrave, *J. Mol. Spectrosc.* **1973**, *45*, 420.
[36] a) M. K. Y. Chan, G. Ceder, *Phys. Rev. Lett.* **2010**, *105*, 196403; b) P. J. Hasnip, K. Refson, M. I. J. Probert, J. R. Yates, S. J. Clark, C. J. Pickard, *Philos. T. R. Soc. A.* **2014**, *372*, 20130270.
[37] a) G. Zou, C. Lin, H. Jo, G. Nam, T. S. You, K. M. Ok, *Angew. Chem., Int. Ed.* **2016**, *55*, 12078; b) E. J. Cho, S. J. Oh, H. Jo, J. Lee, T. S. You, K. M. Ok, *Inorg. Chem.* **2019**, *58*, 2183; c) Y. Liu, Y. Gong, S. Geng, M. Feng, D. Manidaki, Z. Deng, C. C. Stoumpos, P. Canepa, Z. Xiao, W. Zhang, L. Mao, *Angew. Chem., Int. Ed.* **2022**, *61*, e202208875.
[38] a) H. Tan, F. Che, M. Wei, Y. Zhao, M. I. Saidaminov, P. Todorovic, D. Broberg, G. Walters, F. Tan, T. Zhuang, B. Sun, Z. Liang, H. Yuan, E. Fron, J. Kim, Z. Yang, O. Voznyy, M. Asta, E. H. Sargent, *Nat. Commun.* **2018**, *9*, 3100; b) J. M. Frost, K. T. Butler, F. Brivio, C. H. Hendon, M. Van Schilfgaarde, A. Walsh, *Nano Lett.* **2014**, *14*, 2584.